*Inorg. Chem.* **2007**, *46*, 7610–7620


# Selective Oxidation and Reduction of Trinuclear Titanium(II) Hexaazatrinaphthylene Complexes—Synthesis, Structure, and Electrochemical Investigations

**Ingmar M. Piglosiewicz, RUdiger Beckhaus,* Gunther Wittstock, Wolfgang Saak, and Detlef Haase**

*Institute for Pure and Applied Chemistry, University of Oldenburg, D-26111 Oldenburg, Germany*

Received May 24, 2007

Titanocene complexes with chelating *N*-heterocyclic ligand bridges react with ferrocenium salts as selective oxidants to afford air-stable cationic complexes and allow the preparation of exceptional mixed valence hexaazatrinaphthylene complexes $[(Cp_2Ti)_3(\mu_3\text{-HATNMe}_6)]^{n+}$ ($\mathbf{1}^{n+}$) ($n$ = 1, 2, 3, 4). Cyclic voltammograms (CV) and differential pulse voltammograms (DPV) show that nine oxidation states of **1** are generated without decomposition. Comproportionation constants $K_c$ have been calculated in order to determine the extent of electronic communication between the titanium centers. The $K_c$ values of the mixed valence states are indicative of uncoupled ($\mathbf{1}^{4+}$), moderately coupled ($\mathbf{1}^{5+}$), and strongly coupled ($\mathbf{1}^{-}$, $\mathbf{1}^{+}$, and $\mathbf{1}^{2+}$) systems. Small but significant structural changes occurring upon oxidation of neutral **1** are observed by X-ray structural analysis on $\mathbf{1}^{+}$–$\mathbf{1}^{4+}$. Anion–$\pi$ interactions between the electron-deficient central ring of the $HATNMe_6$ moiety and $PF_6^-$ and $BF_4^-$ counterions, respectively, are found for $\mathbf{1}^{2+}$, $\mathbf{1}^{3+}$, and $\mathbf{1}^{4+}$. The short cation–anion contacts cause interesting molecular allignments in terms of molecular architecture. For $\mathbf{1}^{2+}$ the assembly of an one-dimensional (1D) polymer is observed. Electrochemical investigations on the mononuclear cationic titanocene complexes $[(Cp_2Ti)(L)]^+$ (L = 2,2′-biquinoline ($\mathbf{2}^+$), 4,4′-dimethyl-2,2′-biquinoline ($\mathbf{3}^+$), and 5,8′-dimethyl-2,3′-biquinoxaline ($\mathbf{4}^+$)) showed similar oxidation and reduction characteristics among each other. Conversion to monoanionic, neutral, and dicationic states is enabled. As found for the trinuclear compounds $\mathbf{1}^{n+}$, the molecular structures of $\mathbf{2}^+$–$\mathbf{4}^+$ reveal significant differences compared to their neutral parents.

## Introduction

The trischelating nitrogen heterocyclic molecule 1,4,5,8,9,12-hexaazatriphenylene (HAT)[1a] and its homologues, for example 1,6,7,12,13,18-hexaazatrinaphthylene (HATN)[1b] or its hexamethyl derivative ($HATNMe_6$),[1c] were often studied in the context of their coordination modes to metal ions,[2] photophysical properties,[3] liquid crystalline ordering,[4] light-harvesting systems,[5] chirality,[6] and DNA related chemistry.[7] The molecular symmetry of HAT and HATN derivatives leads to especially interesting building blocks creating self-assembled 3D frameworks.[8] Additionally, nonporous network polymers become available from HATN derivatives,[9] including polymer-based hydrogen storage materials.[9c] Employing paramagnetic metal centers in HAT- and HATN-type

* To whom correspondence should be addressed. E-mail: ruediger.beckhaus@uni-oldenburg.de.

(1) (a) Grove, H.; Sletten, J. *J. Chem. Crystallogr.* **2000**, *30*, 123−130. (b) Alfonso, M.; Stoeckli-Evans, H. *Acta Crystallogr., Sect. E: Struct. Rep. Online* **2001**, *E57*, o242−o244. (c) Catalano, V. J.; Larson, W. E.; Olmstead, M. M.; Gray, H. B. *Inorg. Chem.* **1994**, *34*, 4502−4509.

(2) (a) Browne, W. R.; Hage, R.; Vos, J. G. *Coord. Chem. Rev.* **2006**, *250*, 1653−1668. (b) Kitagawa, S.; Masaoka, S. *Coord. Chem. Rev.* **2003**, *246*, 73−88. (c) Keene, F. R. *Coord. Chem. Rev.* **1997**, *166*, 121−159.

(3) (a) Ishi-I, T.; Yaguma, K.; Kuwahara, R.; Taguri, Y.; Mataka, S. *Org. Lett.* **2006**, *8*, 585−588. (b) Herrera, J.-M.; Ward, M. D.; Adams, H.; Pope, S. J. A.; Faulkner, S. *Chem. Commun.* **2006**, 1851−1853. (c) Didier, P.; Ortmans, I.; Kirsch-De Mesmaeker, A.; Watts, R. J. *Inorg. Chem.* **1993**, *32*, 5239−5245. (d) Rutherford, T. J.; Van Gijte, O.; Kirsch-De Mesmaeker, A.; Keene, F. R. *Inorg. Chem.* **1997**, *36*, 4465−4474.

(4) (a) Ishi-i, T.; Hirayama, T.; Murakami, K.-I.; Tashiro, H.; Thiemann, T.; Kubo, K.; Mori, A.; Yamasaki, S.; Akao, T.; Tsuboyama, A.; Mukaide, T.; Ueno, K.; Mataka, S. *Langmuir* **2005**, *21*, 1261−1268. (b) Chang, T.-H.; Wu, B.-R.; Chiang, M. Y.; Liao, S.-C.; Ong, C. W.; Hsu, H.-F.; Lin, S.-Y. *Org. Lett.* **2005**, *7*, 4075−4078. (c) Lehmann, M.; Kestemont, G.; Aspe, R. G.; Buess-Herman, C.; Koch, M. H. J.; Debije, M. G.; Piris, J.; de Haas, M. P.; Warman, J. M.; Watson, M. D.; Lemaur, V.; Cornil, J.; Geerts, Y. H.; Gearba, R.; Ivanov, D. A. *Chem.—Eur. J.* **2005**, *11*, 3349−3362. (d) Lemaur, V.; da Silva, F.; Demetrio, A.; Coropceanu, V.; Lehmann, M.; Geerts, Y.; Piris, J.; Debije, M. G.; van de Craats, A. M.; Senthilkumar, K.; Siebbeles, L. D. A.; Warman, J. M.; Bredas, J.-L.; Cornil, J. *J. Am. Chem. Soc.* **2004**, *126*, 3271−3279.

(5) (a) Ishi-i, T.; Murakami, K.-I.; Imai, Y.; Mataka, S. *J. Org. Chem.* **2006**, *71*, 5752−5760. (b) Ishi-i, T.; Murakami, K.; Imai, Y.; Mataka, S. *Org. Lett.* **2005**, *7*, 3175−3178.



10.1021/ic701009u CCC: $37.00 
Published on Web 07/21/2007

complexes, magnetic properties of those derivatives,[10] including spin-frustrated behavior or antiferromagnetic couplings, are of interest.[11]

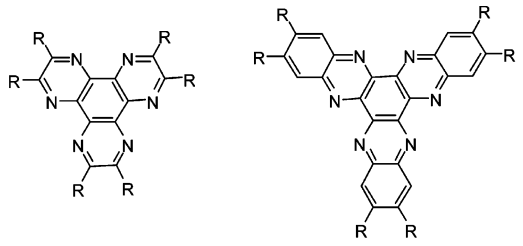

1,4,5,8,9,12-Hexaazatriphenylene (**HAT**)

1,6,7,12,13,18-Hexaazatrinaphthylene (R = H, **HATN**; R = $CH_3$ **HATNMe$_6$**)

Electron and energy transfer are ubiquitous in chemical, physical, and biological processes.[12] In particular, intramolecular electron-transfer reactions within polymetallic assemblies are of considerable importance. Starting with the preparation of the Creutz−Taube ion (**A**),[13] polypyridyl complexes of the $d^6$ metals $Fe^{II}$, $Ru^{II}$, and $Os^{II}$ have received considerable attention due to their chemical inertness in a variety of oxidation states.

The most obvious manifestation of metal−metal interactions is a separation of the redox potentials of the metal-centered electron-transfer processes occurring at chemically equivalent metals of the same molecule.[14] So far, intensive

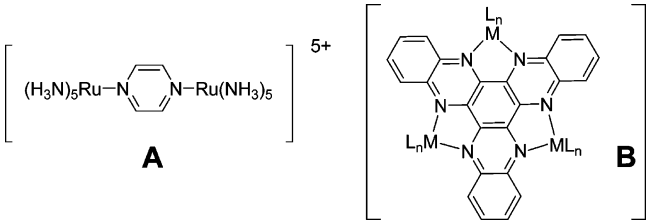

**A** **B**

research on metal−metal interaction has been carried out using late transition metals. However, HAT as well as HATN derivatives are interesting ligands for different applications in chemistry, but due to the low solubility and the laborious synthesis[15] they have not been explored as extensively as other chelating nitrogen-containing heterocycles. So far, discrete homonuclear $M_3(\mu_3$-HAT) ensembles are known for Cr(0),[16] Cu(I),[8b] Ru(II),[3c,3d,17] Rh(III),[17] Fe(II),[11] and Ti(II).[18] A few heterometallic $MM'_2(\mu_3$-HAT) molecules containing $Ru_2Os$,[19] $Ru_2Rh$, and $RuRh_2$[17] have been prepared. On the other hand, HATN has an advantage over HAT because it is the condensation product of two commercially available reagents.[20] However, the number of comparable HATN derivatives (**B**) known is still low.[1,8a,21,22] Often only one or two chelate positions of the HATN ligand are occupied. Herein, we report the synthesis, structure, and electrochemical properties of novel cationic trinuclear titanium $HATNMe_6$ complexes, which can be obtained by stepwise oxidation of $(Cp_2Ti)_3(\mu_3$-$HATNMe_6)$ (**1**)[21] derivatives employing ferrocenium salts. Ferrocenium salts are well established as selective one-electron oxidation agents in organometallic as well as coordination chemistry.[23,24]

## Results and Discussion

**Synthesis of [$(Cp_2Ti)_3(\mu_3$-$HATNMe_6)$] Cations.** Complexation of titanocene(II) fragments, generated from the


(6) (a) Abrahams, B. F.; Jackson, P. A.; Robson, R. *Angew. Chem.* **1998**, *110*, 2801−2804; Abrahams, B. F.; Jackson, P. A.; Robson, R. *Angew. Chem., Int. Ed. Engl.* **1998**, *37*, 2656−2659. (b) Rutherford, T. J.; Keene, F. R. *J. Chem. Soc., Dalton Trans.* **1998**, 1155−1162.

(7) (a) Smith, J. A.; Morgan, J. L.; Turley, A. G.; Collins, J. G.; Keene, F. R. *Dalton Trans.* **2006**, 3179−3187. (b) Angeles-Boza, A. M.; Bradley, P. M.; Fu, P. K.-L.; Shatruk, M.; Hilfiger, M. G.; Dunbar, K. R.; Turro, C. *Inorg. Chem.* **2005**, *44*, 7262−7264. (c) Furukawa, S.; Okubo, T.; Masaoka, S.; Tanaka, D.; Chang, H.-C.; Kitagawa, S. *Angew. Chem.* **2005**, *117*, 2760−2764; Furukawa, S.; Okubo, T.; Masaoka, S.; Tanaka, D.; Chang, H.-C.; Kitagawa, S. *Angew. Chem., Int. Ed.* **2005**, *44*, 2700−2704. (d) Kaafarani, B. R.; Kondo, T.; Yu, J.; Zhang, Q.; Dattilo, D.; Risko, C.; Jones, S. C.; Barlow, S.; Domercq, B.; Amy, F.; Kahn, A.; Bredas, J.-L.; Kippelen, B.; Marder, S. R. *J. Am. Chem. Soc.* **2005**, *127*, 16358−16359. (e) Van Gijte, O.; Kirsch-De Mesmaeker, A. *J. Chem. Soc., Dalton Trans.* **1999**, 951−956. (f) Lecomte, J.-P.; Kirsch-De Mesmaeker, A.; Feeney, M. M.; Kelly, John M. *Inorg. Chem.* **1995**, *34*, 6481−6489. (g) Moucheron, C.; Kirsch-De Mesmaeker, A.; Choua, S. *Inorg. Chem.* **1997**, *36*, 584−592.

(8) (a) Bu, X.-H.; Tanaka, K.; Shionoya, M.; Biradha, K.; Yamaguchi, T.; Nishimura, M.; Ito, T. *J. Chem. Soc., Chem. Commun.* **2000**, 1953−1954. (b) Baxter, P. N. W.; Lehn, J.-M.; Baum, G.; Fenske, D. *Chem.−Eur. J.* **1999**, *5*, 102−112. (c) Baxter, P. N. W.; Lehn, J.-M.; Baum, G.; Fenske, D. *Chem.−Eur. J.* **1999**, *5*, 113−120. (d) Pérez, D.; Guitián, E. *Chem. Soc. Rev.* **2004**, *33*, 274−283.

(9) (a) Budd, P. M.; Ghanem, B.; Msayib, K.; McKeown, N. B.; Tattershall, C. *J. Mater Chem.* **2003**, *13* (11), 2721−2726. (b) Bushby, R. J.; Hamley, I. W.; Liu, Q.; Lozman, O. R.; Lydon, J. E. *J. Mater. Chem.* **2005**, *15*, 4429−4434. (c) McKeown, N. B.; Gahnem, B.; Msayib, K. J.; Budd, P. M.; Tattershall, C. E.; Mahmood, K.; Tan, S.; Book, D.; Langmi, H. W.; Walton, A. *Angew. Chem.* **2006**, *116*, 1836−1839; McKeown, N. B.; Gahnem, B.; Msayib, K. J.; Budd, P. M.; Tattershall, C. E.; Mahmood, K.; Tan, S.; Book, D.; Langmi, H. W.; Walton, A. *Angew. Chem., Int. Ed.* **2006**, *45*, 1804−1807.

(10) (a) Galan-Mascaros, J. R.; Dunbar, K. R. *Chem. Commun.* **2001**, 217−218. (b) Marshall, S. R.; Rheingold, A. L.; Dawe, L. N.; Shum, W. W.; Kitamura, C.; Miller, J. S. *Inorg. Chem.* **2002**, *41*, 3599−3601.

(11) Shatruk, M.; Chouai, A.; Prosvirin, A. V.; Dunbar, K. R. *Dalton Trans.* **2005**, 1897−1902.

(12) D'Alessandro, D. M.; Keene, F. R. *Chem. Rev.* **2006**, *106*, 2270−2298.

(13) Creutz, C.; Taube, H. *J. Am. Chem. Soc.* **1973**, *95*, 1086−1094.

(14) Kaim, W.; Lahiri, G. K. *Angew. Chem.* **2007**, *119*, 1808−1828; Kaim, W.; Lahiri, G. K. *Angew. Chem., Int. Ed.* **2007**, *46*, 1778−1796.

(15) (a) Sarma, M. S. P.; Czarnik, A. W. *Synthesis* **1988**, 72−73. (b) Rademacher, J. T.; Kanakarajan, K.; Czarnik, A. W. *Synthesis* **1994**, 378−380.

(16) Nasielski-Hinkens, R.; Benedek-Vamos, M.; Maetens, D.; Nasielski, J. *J. Organomet. Chem.* **1981**, *217*, 179−182.

(17) Didier, P.; Jacquet, L.; Kirsch-De Mesmaeker, A.; Hueber, R.; Van Dorsselaer, A. *Inorg. Chem.* **1992**, *31*, 4803−4809.

(18) Instead of a central benzene ring, a cyclohexane moiety is formed due to the special synthetic route. Kraft, S.; Beckhaus, R.; Haase, D.; Saak, W. *Angew. Chem.* **2004**, *116*, 1609−1614; Kraft, S.; Beckhaus, R.; Haase, D.; Saak, W. *Angew. Chem., Int. Ed.* **2004**, *43*, 1583−1587.

(19) Rutherford, T. J.; Keene, F. R. *Inorg. Chem.* **1997**, *36*, 3580−3581.

(20) (a) Skujins, S.; Webb, G. A. *Tetrahedron* **1969**, *25* (17), 3935−3945. (b) Farminer, A. R.; Skujins, S.; Webb, G. A. *J. Mol. Struct.* **1971**, *10* (1), 121−34.

(21) Piglosiewicz, I.; Beckhaus, R.; Saak, W.; Haase, D. *J. Am. Chem. Soc.* **2005**, *127*, 14190−14191.

(22) (a) Du, M.; Bu, X.-H.; Biradha, K.; Shionoya, M. *J. Chem. Res., Synop.* **2002**, *10*, 493−495. (b) Patra, S.; Sarkar, B.; Ghumaan, S.; Fiedler, J.; Kaim, W.; Lahiri, G. K. *J. Chem. Soc., Dalton Trans.* **2004**, *5*, 754−758.

(23) Connelly, N. G.; Geiger, W. E. *Chem. Rev.* **1996**, *96*, 877−910.

(24) (a) Bouwkamp, M. W.; de Wolf, J.; del Hierro Morales, I.; Gercama, J.; Meetsma, A.; Troyanov, S. I.; Hessen, B.; Teuben, J. H. *J. Am. Chem. Soc.* **2002**, *124*, 12956−12957. (b) Jordan, R. F.; LaPointe, R. E.; Bajgur, C. S.; Echols, S. F.; Willett, R. *J. Am. Chem. Soc.* **1987**, *109*, 4111−4113. (c) Calderazzo, F.; Pampaloni, G.; Rocchi, L.; Englert, U. *Organometallics* **1994**, *13*, 2592−2601. (d) Schumann, H. *J. Organomet. Chem.* **1986**, *304*, 341−351. (e) Calderazzo, F.; Ferri, I.; Pampaloni, G.; Englert, U.; Green, M. L. H. *Organometallics* **1997**, *16*, 3100−3101. (f) Calderazzo, F.; Pampaloni, G.; Tripepi, G. *Organometallics* **1997**, *16*, 4943−4944. (g) Caselli, A.; Solari, E.; Scopelliti, R.; Floriani, C. *J. Am. Chem. Soc.* **2000**, *122*, 538−539.

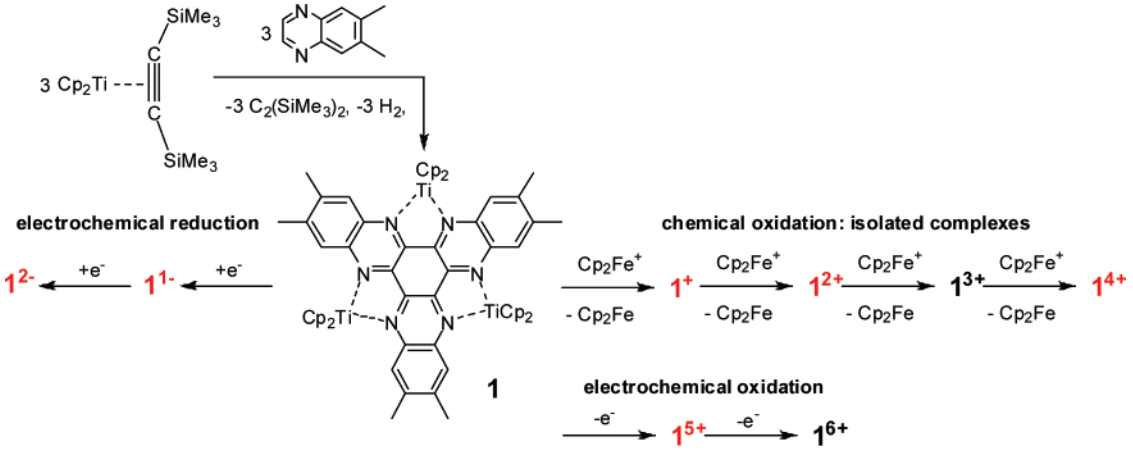


**Figure 1.** Synthesis of **1** by dehydrogenative coupling of 6,7-dimethylquinoxaline. Chemical and electrochemical conversion of **1** (mixed valence states are highlighted).

corresponding bis(trimethylsilyl)acetylene derivative [$Cp_2Ti(\eta^2\text{-}C_2(SiMe_3)_2]$,[25] by $HATNMe_6$ ligands as well as by the dehydrogenative coupling of 6,7-dimethylquinoxaline[21] leads to the highly reactive [$(Cp_2Ti)_3(\mu_3\text{-}HATNMe_6)$] complex (**1**), one of the rare examples in which three metal centers are chelated by HAT-type ligands. Complexation of metal fragments with reducing properties may balance the electron deficiency of the aromatic core and increases the coordination ability of the threefold chelating ligand.[26] Along with the assembly of three $d^2$ centers around a $\mu_3$-bridging aromatic ligand, a six-electron system is created that governs the reactivity. Utilization of suitable oxidants enables a stepwise abstraction of electrons in well separated one-electron oxidation steps. In this manner, cationic complexes $\mathbf{1}^{n+}$ ($n = 1-4$) can be synthesized by adding to the neutral complex **1** stoichiometric amounts of ferrocenium salts as one-electron oxidants. Further oxidation giving rise to complexes $\mathbf{1}^{5+}$ and $\mathbf{1}^{6+}$ can be electrochemically achieved. Electrochemical reduction is also possible, giving $\mathbf{1}^{n-}$ ($n = 1, 2$) (see Figure 1). All preparative reactions proceed at ambient temperature leading to air-stable amorphous or microcrystalline compounds in good yields. Whereas $\mathbf{1}^{+}$, $\mathbf{1}^{2+}$, and $\mathbf{1}^{3+}$ are obtained as analytically pure powders, $\mathbf{1}^{4+}$ is only obtained together with $\mathbf{1}^{3+}$ even if an excess of oxidant is used. This might be expected since the formal potential $E_{1/2}(\mathbf{1}^{3+}/\mathbf{1}^{4+})$ is close to the formal potential of ferrocene/ferrocenium $E_{1/2}(Fc/Fc^{+})$. The mixed valence complexes $\mathbf{1}^{2-}$, $\mathbf{1}^{-}$, $\mathbf{1}^{+}$, $\mathbf{1}^{2+}$, $\mathbf{1}^{4+}$, $\mathbf{1}^{5+}$ are part of a series of structurally comparable compounds. This gives the opportunity of a systematic study on mixed valence complexes of the early transition metal titanium, keeping in mind that this field of chemistry is basically focused on late transition metals. However, a few examples of mixed valence titanium complexes are given.[27−29] Halides,[27b,e,28] $\mu$-oxo units,[27c,d] benzoquinone,[27f] nitrogen,[29a] and toluene[29b] have been employed as bridging ligands.

The reactions are performed in common aliphatic solvents such as *n*-hexane and tetrahydrofuran (THF). When the solvent is added to the reactants, a dark brown solution of the well soluble complex **1** is formed initially. The ferrocenium salt is nearly insoluble and thus reacts slowly. Nevertheless, the occurrence of a reaction can already be observed within the first minutes of stirring the mixture. Light-colored amorphous or microcrystalline solids increasingly precipitate while the solution brightens. After having stirred the respective reaction mixture overnight, the reaction is completed and a homogeneous product could be isolated by filtration. Resulting filtrates are yellow in color due to dissolved ferrocene formed during the course of the reactions. The titanium-containing cationic products are well soluble in acetone, moderately soluble in THF and acetonitrile, but insoluble in nonpolar solvents. The trinuclear complexes $\mathbf{1}^{n+}$ are found to be green ($\mathbf{1}^{+}$), yellow to orange ($\mathbf{1}^{2+}$, $\mathbf{1}^{4+}$), and orange ($\mathbf{1}^{3+}$), respectively. Depending on the nature of the counterions, the crystallization characteristics of the complexes vary. In order to obtain suitable crystals for X-ray structural analysis, ferrocenium salts with the anions $PF_6^-$, $BF_4^-$, and $BPh_4^-$ have been employed in the oxidation reactions. Iodine can also be used as a selective oxidant.

**Mononuclear Complexes.** The properties of mixed valence complexes are often compared to those of related mononuclear "fragments". Depending on the extent of electronic communication in multinuclear assemblies, the chemical and physical behaviors may be very similar or diverge from a monomeric system. Such comparisons

(25) Rosenthal, U.; Burlakov, V. V.; Arndt, P.; Baumann, W.; Spannenberg, A. *Organometallics* **2003**, *22*, 884−900.
(26) Okubo, T.; Kitagawa, S.; Kondo, M.; Matsuzaka, H.; Ishii, T. *Angew. Chem.* **1999**, *111* (7), 980−983; Okubo, T.; Kitagawa, S.; Kondo, M.; Matsuzaka, H.; Ishii, T. *Angew. Chem., Int. Ed.* **1999**, *38* (7), 931−933.
(27) Ti(III)/Ti(IV),[27] Ti(II)/Ti(III),[28] and Ti(I)/Ti(II).[29] (a) Kristine, F. J.; Shepherd, R. E. *Inorg. Chem.* **1981**, *20*, 215−222. (b) Maya, L. *Inorg. Chem.* **1986**, *25*, 4213−4217. (c) Bodner, A.; Vedova, B. S. P. C. D.; Wieghardt, K.; Nuber, B.; Weiss, J. *J. Chem. Soc., Chem. Commun.* **1990**, 1042−1043. (d) Bodner, A.; Jeske, P.; Weyhermüller, T.; Wieghardt, K.; Dubler, E.; Schmalle, H.; Nuber, B. *Inorg. Chem.* **1992**, *31*, 3737−3748. (e) Chen, L.; Cotton, F. A. *Inorg. Chim. Acta* **1998**, *267* (2), 271−279. (f) Calderazzo, F.; Englert, U.; Pampaloni, G.; Passarelli, V. *J. Chem. Soc., Dalton Trans.* **2001**, 2891−2898.
(28) Cotton, F. A.; Murillo, C. A.; Petrukhina, M. A. *J. Organomet. Chem.* **2000**, *593*−*594*, 1−6.
(29) (a) Duchateau, R.; Gambarotta, S.; Beydoun, N.; Bensimon, C. *J. Am. Chem. Soc.* **1991**, *113*, 8986−8988. (b) Nikiforov, G. B.; Crewdson, P.; Gambarotta, S.; Korobkov, I.; Budzelaar, P. H. M. *Organometallics* **2007**, *26*, 48−55.

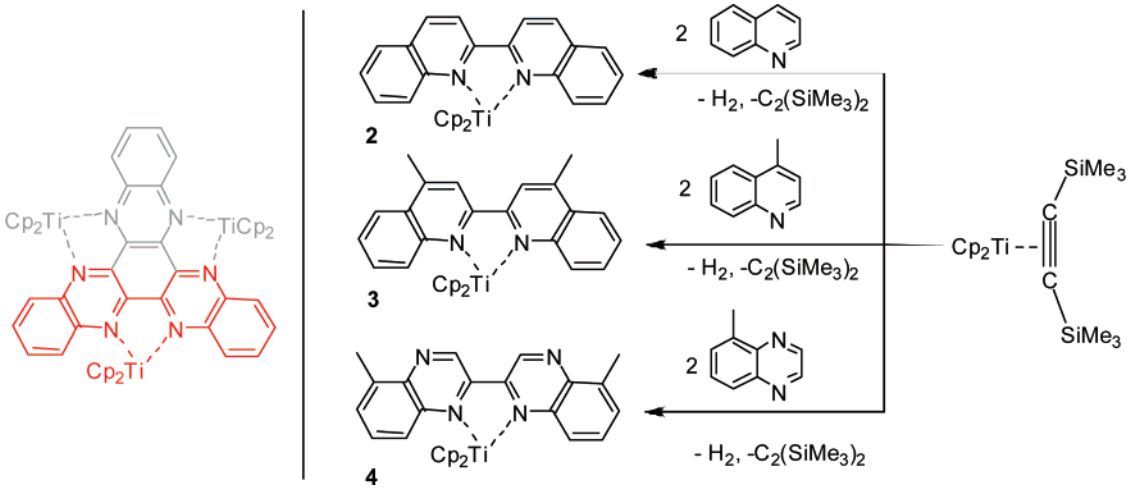


**Figure 2.** Synthesis of **2**−**4** and structural relationship between trinuclear and mononuclear titanocene complexes. 2,2′-Biquinoline and 2,2′-biquinoxaline complexes **2**−**4** as monomeric subunits of the HATN assembly.

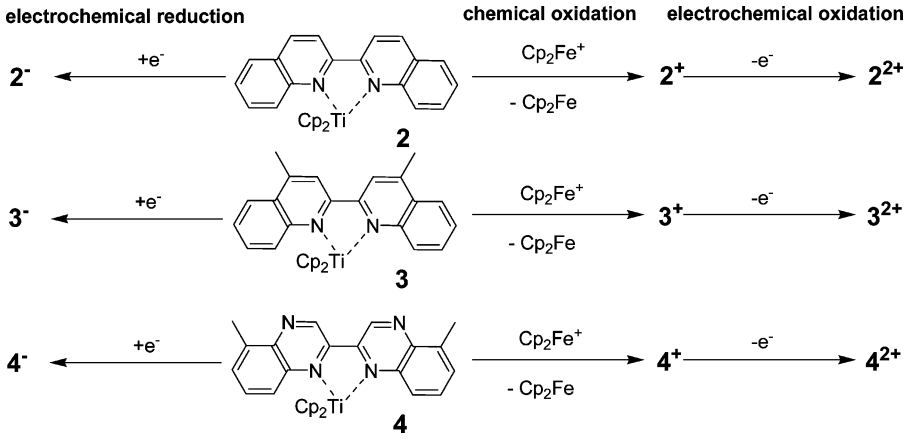


**Figure 3.** Chemical and electrochemical conversion of **2**, **3,** and **4**.

provide information about the properties that arise from metal−metal interaction. In this context, mononuclear 2,2′-biquinoline and 2,2′-biquinoxaline complexes **2**−**4** have been synthesized as monomeric analogues of HATN-assemblies. The structural relation is depicted in Figure 2. The monomeric compounds **2, 3, and 4** are synthesized by dehydrogenative coupling of quinoline, 4-methylquinoline, and 5-methylquinoxaline, respectively.[21,30] These neutral complexes are highly sensitive against air and moisture. They are isolated as dark crystalline, nearly black solids in good yields. Since the heterocylic ligands are coordinated to titanocene as a $d^2$ species, the removal of two electrons should be feasible by utilization of capable oxidants. The cations $\mathbf{2}^+$−$\mathbf{4}^+$ are obtained by addition of 1 equiv of ferrocenium salts to stirred solutions of the corresponding neutral complexes **2**−**4** . The reaction conditions are chosen very similar to those used for the syntheses of the trinuclear compounds $\mathbf{1}^{n+}$ described above. Reactions proceed at ambient temperature within several hours. During the course of the reactions cations $\mathbf{2}^+$−$\mathbf{4}^+$ precipitate as air-stable green powders.

The green color of the monometallic complexes $\mathbf{2}^+$−$\mathbf{4}^+$ is characteristic for Ti(III) compounds. Their $^1$H NMR spectra in acetone-$d_6$ do not exhibit signals in the usual frequency range indicating a paramagnetic nature of $\mathbf{2}^+$−$\mathbf{4}^+$. Further, oxidation to $\mathbf{2}^{2+}$−$\mathbf{4}^{2+}$ as well as a reduction of **2**−**4** to $\mathbf{2}^-$−$\mathbf{4}^-$ is feasible electrochemically (Figure 3). Attempts to synthesize $\mathbf{2}^{2+}$−$\mathbf{4}^{2+}$ employing oxidants with higher oxidation potentials such as [NO][$PF_6$] (0.87 V vs $Fc/Fc^+$)[23] resulted in the release of the respective ligand. The complexation of titanocene dications $[Cp_2Ti]^{2+}$ [31a] has been described for 2,2′-bipyridine and phenanthroline.[31b] However, we were not able to observe similar reactions using 2,2′-biquinolines and 2,2′-biquinoxalines. With iodine as another common oxidant, conversion of **2** to $\mathbf{2}^+$ and triiodide as a counterion is observed (Figure 4). $\mathbf{2}^+\mathbf{I}_3^-$ is readily prepared by addition of 1.5 equiv of iodine in toluene to a solution of the neutral complex **2**. Within several minutes of stirring the mixture, the product precipitates as a greenish powder whereupon the solution completely decolors. The formal potential of the $I^-/I_3^-$ couple is not high enough to enable further oxidation to the corresponding Ti(IV) complex. This is in agreement with the electrochemical investigations ($E_{1/2}$-($\mathbf{2}^+/\mathbf{2}^{2+}$) = −0.10 V vs $Fc/Fc^+$; $E_{1/2}(I/I^-)$ = −0.14 V vs $Fc/Fc^+$.[23]).

(30) Further details are given in the Supporting Information.

(31) (a) Luinstra, G. A. *J. Organomet. Chem.* **1996**, *517*, 209−215. (b) Thewalt, U.; Berhalter, K. *J. Organomet. Chem.* **1986**, *302*, 193−200.

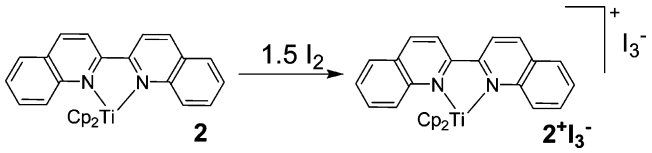


**Figure 4.** Oxidation of the 2,2′-biquinoline complex (**2**) with iodine. Formation of monocation ($\mathbf{2}^{+}$) with triiodide as counterion.

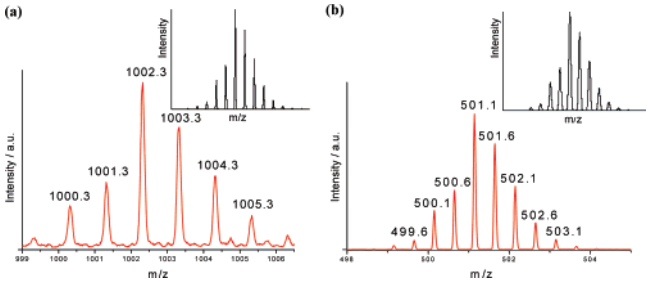


**Figure 5.** ESI-MS investigations: Isotope patterns of $\mathbf{1}^{+}$ (a) and $\mathbf{1}^{2+}$ (b); calculated patterns are given in the insets.

**Sensitivity of Mono- and Trinuclear Complexes.** On comparison to Ti(II) complexes that are known to be highly air sensitive, the stability of the trinuclear complexes $\mathbf{1}^{+}$ and $\mathbf{1}^{2+}$ is exceptional. $\mathbf{1}^{+}$ and $\mathbf{1}^{2+}$ can be formally recognized as ($Ti^{II}_{2}Ti^{III}_{1}$) and ($Ti^{II}_{1}Ti^{III}_{2}$) systems, respectively. The high degree of electron delocalization, as evidenced by the corresponding comproportionation constants $K_c$, seems to push the redox potentials to unusual high values (Table 3). The stability of the mononuclear titanium complexes against air is in agreement with the electrochemical investigations and with the fact that triiodide as a stronger oxidant than oxygen is stable in the presence of $\mathbf{2}^{+}$.

In addition to the electrochemical and crystallographic characterization of the cationic complexes $\mathbf{1}^{n+}$ and $\mathbf{2}^{+}$–$\mathbf{4}^{+}$ the ESI-MS technique was also used. The spectra of the mononuclear complexes $\mathbf{2}^{+}$–$\mathbf{4}^{+}$ show the signals of their respective cationic complexes (positive scan) and the signals arising from the counterion (negative scan).[30] The trinuclear compounds $\mathbf{1}^{+}$, $\mathbf{1}^{2+}$, and $\mathbf{1}^{3+}$ appear to be not fully stable under ESI conditions. However, molecular peaks of these compounds were found. ESI spectra of $\mathbf{1}^{+}$ and $\mathbf{1}^{2+}$ are given in the Supporting Information. The isotope patterns for $\mathbf{1}^{+}$ and $\mathbf{1}^{2+}$ are in agreement with the calculated ones (Figure 5). Detection of $\mathbf{1}^{3+}$ in the respective acetonitrile solution has been achieved, but the signal was not satisfactorily resolved.

**Molecular Structure of Trinuclear [$(Cp_2Ti)_3(\mu_3$-HATNMe$_6$)] Cations. Crystal Structures of $\mathbf{1}^{n+}$.** Suitable crystals for X-ray structure analysis of $\mathbf{1}^{+}$, $\mathbf{1}^{2+}$, $\mathbf{1}^{3+}$, and $\mathbf{1}^{4+}$ were obtained by slow diffusion of *n*-pentane into solutions of the respective complexes in a polar solvent ($\mathbf{1}^{+}$ in THF; $\mathbf{1}^{2+}$, $\mathbf{1}^{3+}$, and $\mathbf{1}^{4+}$ in acetone). The structure details of $\mathbf{1}^{+}$, $\mathbf{1}^{2+}$, $\mathbf{1}^{3+}$ are given in Table 5. The molecular structures ($\mathbf{1}^{+}$–$\mathbf{1}^{3+}$) are presented in Figures 6–8 and that for $\mathbf{1}^{4+}$ is shown in the Supporting Information.[30]

In order to reveal structural changes occurring upon oxidation of **1**, the structures of the oxidation products are compared among themselves as well as to the earlier reported structure of the neutral HATN complex of titanocene.[21]

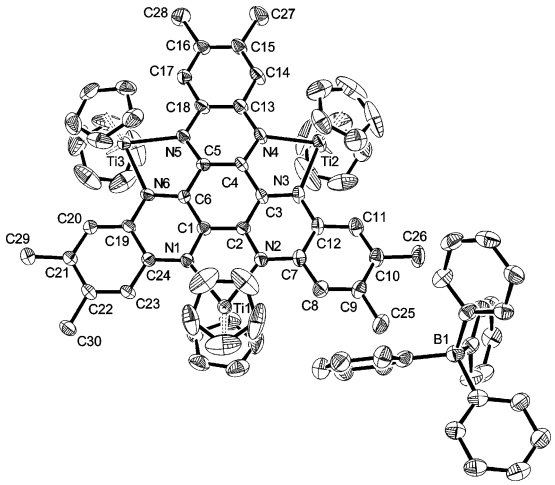


**Figure 6.** Molecular structure of $\mathbf{1}^{+}$ (ORTEP plot with 50% probability thermal ellipsoids, hydrogen atoms are omitted for clarity). Selected bond lengths (Å): Ti1–N1 2.208(4), Ti1–N2 2.223(4), Ti2–N3 2.215(5), Ti2–N4 2.210(4), Ti3–N5 2.210(4), Ti3–N6 2.199(4), N1–C1 1.357(7), N1–C24 1.401(6), N2–C2 1.348(7), N2–C7 1.400(6), N3–C3 1.353(6), N3–C12 1.402(7), N4–C4 1.352(7), N4–C13 1.380(7), N5–C5 1.340(7), N5–C18 1.393(7), N6–C6 1.346(6), N6–C19 1.395(6), C1–C6 1.415(7), C1–C2 1.436(7), C2–C3 1.426(7), C3–C4 1.441(8), C4–C5 1.409(7), C5–C6 1.448(7), C7–C8 1.397(8), C7–C12 1.423(8), C8–C9 1.398(8), C9–C10 1.395(8), C10–C11 1.384(8), C11–C12 1.406(7), C13–C14 1.413(8), C13–C18 1.434(7), C14–C15 1.388(8), C15–C16 1.419(8), C16–C17 1.390(8), C17–C18 1.398(8), C19–C20 1.392(7), C19–C24 1.429(7), C20–C21 1.378(8), C21–C22 1.406(8), C22–C23 1.387(7), C23–C24 1.418(7).

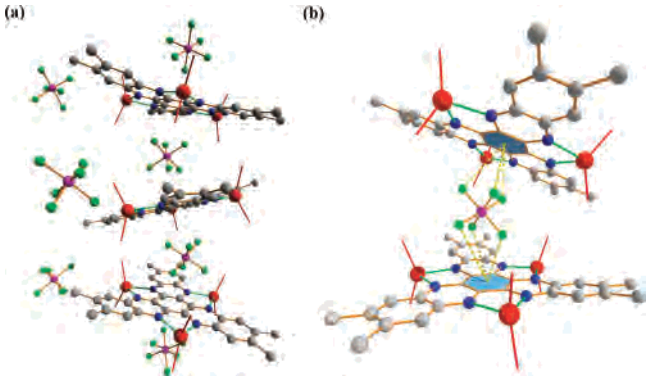


**Figure 7.** Portions of the crystal structure of $\mathbf{1}^{2+}$ (DIAMOND 3.0 plots, hydrogen atoms and cyclopentadienyl rings are omitted for clarity). (a) Packing diagram of $\mathbf{1}^{2+}$ depicting the stacking of $\mathbf{1}^{2+}$ via $PF_6^-$ anions. (b) Anion–$\pi$ interactions between the $PF_6^-$ anions and the $\pi$-acidic central ring of $\mathbf{1}^{2+}$. The dashed lines display the contacts of three fluorine atoms involved in each interaction. The shortest contact between $PF_6^-$ and the centroid of the central $\pi$-ring system is 2.867 Å. The distances between the fluorine atoms and the plane defined by the atoms of the central ring of $\mathbf{1}^{2+}$ range from 2.720 to 3.298 Å. The average distance is 2.905 Å (further structural details for $\mathbf{1}^{2+}$ are given in the Supporting Information).

Structural changes due to electrostatic effects are found to be relatively small since the charge of the cations can be distributed between three metal sites. However, three trends are observed. Oxidation leading to an elongation of the averaged Ti–N bond length, an increase of the averaged Ti–Ti separation, and a contraction of the averaged Ti–$Cp_{centroid}$ distances (Table 1). In all cases, the bridging HATNMe$_6$ ligand maintains planarity and each titanium center resides in a tetrahedral environment.

Depending on the kind of counterion, the trinuclear cations reveal interesting packing in the crystal. Cation $\mathbf{1}^{+}$ has been

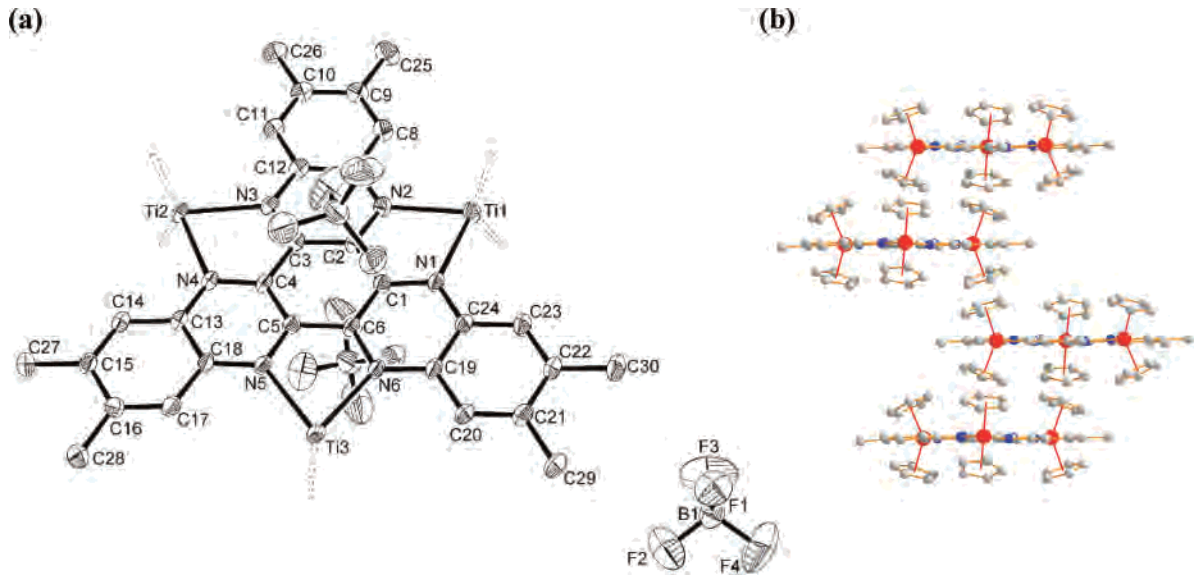


**Figure 8.** (a) Molecular structure of $\mathbf{1}^{3+}$ (ORTEP plot with 50% probability thermal ellipsoids, hydrogen atoms and cyclopentadienyl rings are omitted for clarity). Selected bond lengths (Å): Ti1−N1 2.276(2), Ti1−N2 2.252(2), Ti2−N3 2.239(2), Ti2−N4 2.242(2), Ti3−N5 2.251(2), Ti3−N6 2.277(2), N1−C1 1.330(3), N1−C24 1.373(3), N2−*C*2 1.335(3), N2−C7 1.371(3), N3−C3 1.340(3), N3−C12 1.375(3)N4−C4 1.343(3), N4−C13 1.361(3), N5−C5 1.340(3), C5−C18 1.369(3), N6−C6 1.335(3), N6−C19 1.377(3), C1−C6 1.428(4), C1−C2 1.455(3), C2−C3 1.418(4), C3−C4 1.458(4), C4−C5 1.417(3), C5−C6 1.449(3), C7−C12 1.422(4), C7−C8 1.423(4), C8−C9 1.367(4), C9−C10 1.438(4), C11−C12 1.421(4), C13−C14 1.418(4), C13−C18 1.428(4), C14−C15 1.370(4), C15−C16 1.446(4), C16−C17(1.367(4), C17−C18 1.426(4), C19−C20 1.410(4), C19−C24 1.434(4), C20−C21 1.373(4), C21−C22 1.439(4), C22−C23 1.370(4), C23−C24 1.416(4). The shortest contact between $BF_4^-$ and the centroid of the central $\pi$-ring system is 2.996 Å. (b) Portion of the crystal structure of $\mathbf{1}^{3+}$ (DIAMOND 3.0 plot, hydrogen atoms and $BF_4^-$ counterions are omitted for clarity).

**Table 1.** Selected Averaged Bond Distances and Separations (Å) of Trinuclear Titanocene Complexes

| | $[(Cp_2Ti)_3(\mu_3\text{-HATN})]^a$ | $\mathbf{1}^+$ | $\mathbf{1}^{2+}$ | $\mathbf{1}^{3+}$ |
|---|---|---|---|---|
| Ti−N | 2.183 | 2.210 | 2.242 | 2.256 |
| Ti−Ti | 7.188 | 7.265 | 7.303 | 7.314 |
| $Ti-Cp_{centroid}$ | 2.084 | 2.071 | 2.070 | 2.055 |

[a] Data taken from ref 21.

crystallized with tetraphenylborate as a counterion giving well separated ions (Figure 6). In contrast, the smaller fluorine-containing anions $PF_6^-$ and $BF_4^-$ in $\mathbf{1}^{2+}$ and $\mathbf{1}^{3+}$, respectively, considerably interact with their respective cations. In both cases, anions are located above and beneath the central ring of the $HATNMe_6$ ligand (Figures 7 and 8). Three fluorine atoms are involved in each interaction. Their distance to the plane defined by the atoms of the central ring of the ligand averages 2.905 Å ($\mathbf{1}^{2+}$) and 3.129 Å ($\mathbf{1}^{3+}$). The shortest contacts of the counterions to the centroid of the central $\pi$-ring system are 2.867 ($\mathbf{1}^{2+}$) and 2.996 Å ($\mathbf{1}^{3+}$). This is in a typical range for interactions between anions and $\pi$-electron-deficient aromatic rings described as "anion−$\pi$ interactions".[32] In $\mathbf{1}^{2+}$, half of the $PF_6^-$ anions are sandwiched between two cationic entities. This causes the assembly of a 1D polymer wherein anions and cations alternate. The $HATNMe_6$ units in $\mathbf{1}^{2+}$ are not coplanar. The planes defined by the atoms of the central $\pi$ rings of two superimposed ligands are tilted by 26.1° against each other (Figure 7).

In $\mathbf{1}^{3+}$, two-thirds of the $BF_4^-$ ions are interacting with the central electron-deficient $\pi$ system of the cation preventing a 1D organization. Nevertheless, the packing diagram shows a parallel alignment of all cationic units which cannot be directly ascribed to effects of the anion−$\pi$ interactions (Figure 8b).

**Molecular Structure of Mononuclear Complexes. Crystal Structures of $\mathbf{2}^+$, $\mathbf{3}^+$, and $\mathbf{4}^+$.** Single crystals of $\mathbf{2}^+$ and $\mathbf{3}^+$ were grown by slow diffusion of *n*-pentane into acetone solutions. Very thin crystals of $\mathbf{4}^+$ were obtained by recrystallization from acetone. The molecular structures of the neutral complexes **2**−**4** and the cationic derivative $\mathbf{4}^+$ are given in the Supporting Information.

$\mathbf{2}^+$ has been prepared with the counterions $PF_6^-$ and $I_3^-$ (Figures 9 and 10), respectively. The structural properties are compared to those of the neutral 2,2′-biquinoline complex **2**.[21] The 2,2′-biquinoline chelator in **2** reveals structural properties of a reduced ligand. The reduction is essentially characterized by a shortening of the C−C bond connecting the quinoline units (free ligand, 1.492(3) Å;[33] **2**, 1.432(2) Å). The oxidation of **2** to $\mathbf{2}^+$ leads to a significant elongation of this C−C bond ($\mathbf{2}^+\mathbf{PF_6}^-$, C9−C10 = 1.477(5) Å; $\mathbf{2}^+\mathbf{I_3}^-$, C9−C9′ = 1.484(5) Å). These values closely resemble to that of the free ligand indicating a Ti(III) center coordinated to a nearly unreduced biquinoline ligand. This is in agreement with the color observed (**2**, nontransparent dark crystals; $\mathbf{2}^+$, transparent greenish ($\mathbf{2}^+\mathbf{PF_6}^-$) and transparent brown-green crystals ($\mathbf{2}^+\mathbf{I_3}^-$), both typical for Ti(III) complexes) and studies on the related $[(Cp_2Ti)(2,2'\text{-bipyridine})]^+[PF_6]^-$. The cationic complex $\mathbf{2}^+$ was found to behave as a simple $d^1$ system.[34] The molecular structures of $\mathbf{2}^+$ reveal significantly

(32) (a) Garau, Carolina; Quinonero, David; Frontera, Antonio; Costa, Antoni; Ballester, Pau; Deya, Pere M. *Chem. Phys. Lett.* **2003**, *370*, 7−13. (b) Mascal, M.; Armstrong, A.; Bartberger, M. D. *J. Am. Chem. Soc.* **2002**, *124*, 6274−6276. (c) Demeshko, S.; Dechert, S.; Meyer, F. *J. Am. Chem. Soc.* **2004**, *126*, 4508−4509.

(33) Folting, K.; Merritt, L. L., Jr. *Acta Crystallogr.* **1977**, *B33*, 3540−3542.

(34) McPherson, A. M.; Fieselmann, B. F.; Lichtenberger, D. L.; McPherson, G. L.; Stucky, G. D. *J. Am. Chem. Soc.* **1979**, *101*, 3425−3430.

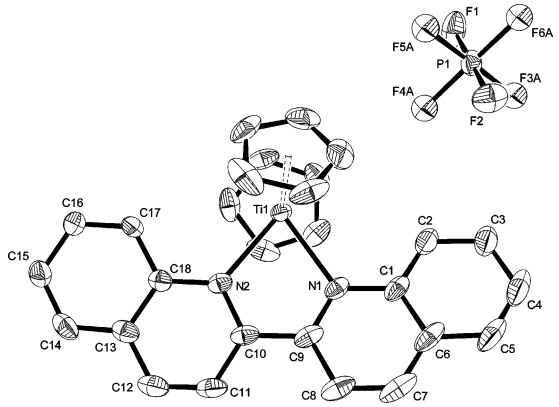


**Figure 9.** Molecular structure of $\mathbf{2}^+$ (ORTEP plot with 50% probability thermal ellipsoids, hydrogen atoms are omitted for clarity). Selected bond lengths (Å): Ti1−N1 2.247(3), Ti1−N2 2.237(3), N1−C9 1.336(4), C1−C1 1.392(4), N2−C10 1.343(4), N2−C18 1.392(4), C1−C2 1.415(5), C1−C6 1.429(5), C2−C3 1.389(5), C3−C4 1.425(6), C4−C5 1.347(7), C5−C6 1.417(6), C6−C7 1.415(6), C7−C8 1.359(6), C8−C9 1.432(5), C9−C10 1.477(5), C10−C11 1.428(5), C11−C12 1.361(5), C12−C13 1.420(5), C13−C14 1.410(5), C13−C18 1.423(5), C14−C15 1.371(5), C15−C16 1.415(5), C16−C17 1.362(5), C17−C18 1.422(4).

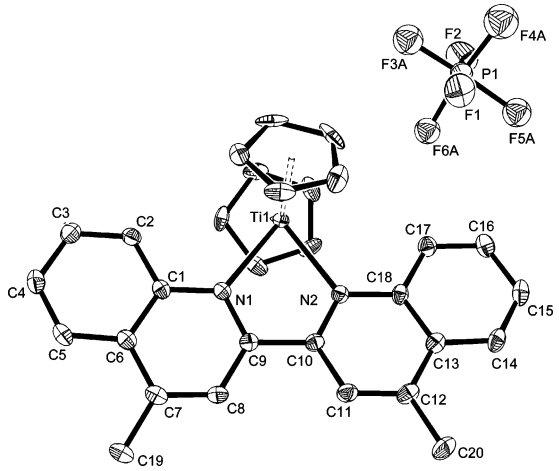


**Figure 10.** Molecular structure of $\mathbf{3}^+$ (ORTEP plot with 50% probability thermal ellipsoids, hydrogen atoms are omitted for clarity). Selected bond lengths (Å): Ti1−N1 2.2523(19), Ti1−N2 2.2445(19), N1−C9 1.340(3), N1−C1 1.391(3), N2−C10 1.338(3), N2−C18 1.395(3), C1−C2 1.421-(3), C1−C6 1.427(3), C2−C3 1.382(3), C3−C4 1.403(4), C4−C5 1.370-(4), C5−C6 1.426(3), C6−C7 1.427(3), C7−C8 1.374(3), C7−C19 1.506(4), C8−C9 1.410(3), C9−C10 1.496(3), C10−C11 1.413(3), C11−C12 1.368(3), C12−C13 1.425(4), C12−C20 1.507(3), C13−C14 1.420-(3), C13−C18 1.427(3), C14−C15 1.373(4), C17−C18 1.420(4), C15−C16 1.418(4), C16−C17 1.378(3).

elongated Ti−N bonds compared to neutral **2**. The Ti−N distances in **2** average 2.194 Å. For $\mathbf{2}^+$, average Ti−N distances of 2.242 Å ($\mathbf{2}^+\mathbf{PF_6}^-$) and 2.2527 Å ($\mathbf{2}^+\mathbf{I_3}^-$) are found. Furthermore, it is observed that the Ti−Cp bonds of the complexes $\mathbf{2}^+\mathbf{PF_6}^-$ (2.071 Å) and $\mathbf{2}^+\mathbf{I_3}^-$ (2.066 Å) are contracted relative to their neutral parent (2.093 Å). The Ti−Cp contraction occurring upon oxidation is also found for the trinuclear compounds described in this paper and is attributed to the electrostatic differences between the redox congeners.

Similar structural changes occurring upon oxidation are found by comparison of **3** and $\mathbf{3}^+$ and of **4** and $\mathbf{4}^+$ (for molecular structure of $\mathbf{3}^+$ see Figure 10; see Supporting Information for structural details of **3**, **4**, and $\mathbf{4}^+$). In the

**Table 2.** Selected Averaged Bond Distances (Å) for Mononuclear Titanocene Complexes

| | C−C[a] | Ti−N | Ti−$Cp_{centroid}$ |
|---|---|---|---|
| 2,2′-**biquinoline**[b] | 1.492(3) | NA | NA |
| **2**[c] | 1.432(2) | 2.194 | 2.093 |
| $\mathbf{2}^+\mathbf{PF_6}^-$ | 1.477(5) | 2.242 | 2.071 |
| $\mathbf{2}^+\mathbf{I_3}^-$ | 1.484(5) | 2.252 | 2.066 |
| **3**[d] | 1.429(2) | 2.187 | 2.092 |
| $\mathbf{3}^+$ | 1.496(3) | 2.248 | 2.081 |
| **4**[d] | 1.428(5) | 2.201 | 2.089 |
| $\mathbf{4}^+$ [d] | 1.470(11) | 2.254 | 2.051 |

[a] C−C bond connecting the quinoline and quinoxaline units. [b] Data taken from ref 33. [c] Data taken from ref 21. [d] See Supporting Information.

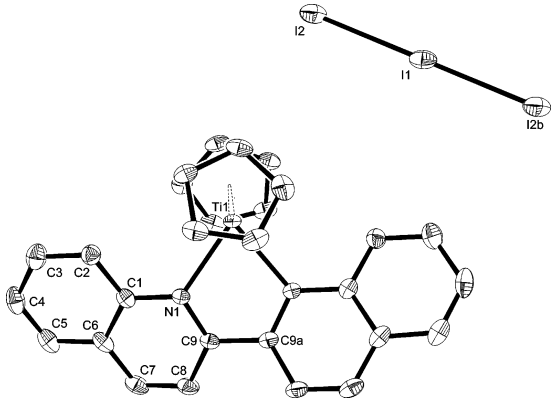


**Figure 11.** Molecular structure of $\mathbf{2}^+\mathbf{I_3}^-$ (ORTEP plot with 50% probability thermal ellipsoids, hydrogen atoms are omitted for clarity). Selected bond lengths (Å): Ti1−N1 2.2527(18), N1−C9 1.337(3), N1−C1 1.386(3), C1−C2 1.418(3), C1−C6 1.425(3), C2−C3 1.373(4), C3−C4 1.414(4), C4−C5 1.362(4), C5−C6 1.422(4), C6−C7 1.416(4), C7−C8 1.362(4), C8−C9 1.414(3), C9−C9′1.484(5), I1−I2 2.9435(2). Symmetry transformation for the generation of equivalent atoms: (a) $-x + 1$, $y$, $-z + 1/2$. (b) $-x + 1$, $-y + 1$, $-z + 1$.

neutral complexes **3** and **4**, the C−C bonds connecting the heterocyclic units appear shorter compared to the respective bonds of free 2,2′-biquinoline (1.429(2) Å (**3**) and 1.428(5) Å (**4**)). These C−C bonds are found to be elongated in the cationic complexes $\mathbf{3}^+$ and $\mathbf{4}^+$ (1.496(3) Å ($\mathbf{3}^+$) and 1.470-(11) Å ($\mathbf{4}^+$)). The values are in the range as found for 2,2′-biquinoline.[33]

The oxidation also leads to contracted Ti−Cp bonds (average values 2.092 Å (**3**), 2.081 Å ($\mathbf{3}^+$) and 2.089 Å (**4**), 2.051 Å ($\mathbf{4}^+$)) and elongated Ti−N bonds (average values 2.187 Å (**3**), 2.248 Å ($\mathbf{3}^+$) and 2.201 Å (**4**), 2.254 Å ($\mathbf{4}^+$)). The structural changes occur for the same reasons as described above for complexes **2** and $\mathbf{2}^+$. Characteristic bond lengths of 2,2′-biquinoline, **2**, $\mathbf{2}^+\mathbf{PF_6}^-$, $\mathbf{2}^+\mathbf{I_3}^-$, **3**, $\mathbf{3}^+$, **4,** and $\mathbf{4}^+$ are summarized in Table 2.

The molecular structure of $\mathbf{2}^+\mathbf{I_3}^-$ exhibits a well separated triiodide ion (Figure 11). The $\mathbf{I_3}^-$ ion is found to be symmetric (I1−I2 = 2.9435(2) Å, I2−I1−I2b = 180.0°), as determined for many other compounds containing this ion.[35] No binding interactions between the triiodide ions can be assumed (shortest interionic I−I distance = 4.565 Å) in contrast to numerous examples where short interionic contacts between polyiodide ions have been documented.[36]

**Electrochemical Behavior of 1−4.** Cyclic voltammograms (CV) and differential pulse voltammograms (DPV)

(35) Svensson, P. H.; Kloo, L. *Chem. Rev.* **2003**, *103*, 1649−1684.

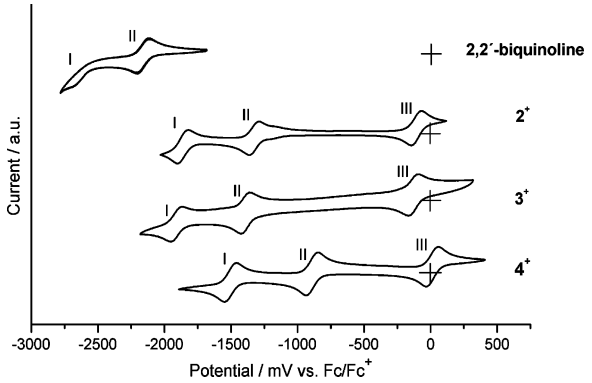


**Figure 12.** Room-temperature voltammograms of 2,2′-biquinoline, $\mathbf{2}^+$, $\mathbf{3}^+$, and $\mathbf{4}^+$ at a Pt disk working electrode in 0.1 M solutions of $[(n\text{-}C_4H_9)_4N][PF_6]$ in acetonitrile. Currents are arbitrary units to facilitate comparison.

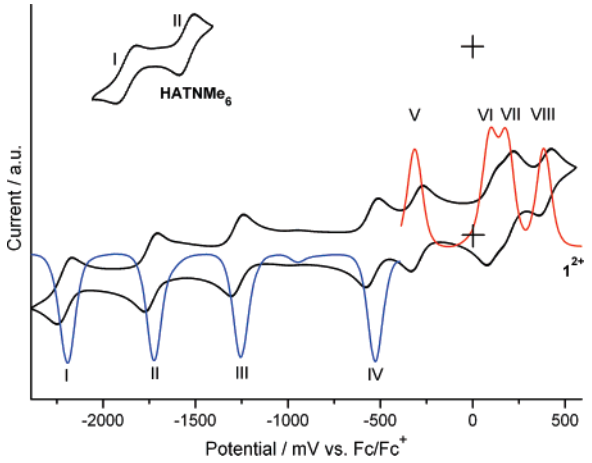


**Figure 13.** CV (black) and DPV (red, blue) of **HATNMe$_6$** and $\mathbf{1}^{2+}$ at a Pt disk working electrode in 0.1 M solutions of $[(n\text{-}C_4H_9)_4N][PF_6]$ in acetonitrile ($\mathbf{1}^{2+}$) and $CH_2Cl_2$ (HATNMe$_6$), respectively. Currents are arbitrary units to facilitate comparison.

of $\mathbf{1}^{2+}$, $\mathbf{2}^+\mathbf{PF_6}^-$, $\mathbf{3}^+$, $\mathbf{4}^+$, 2,2′-biquinoline, and the HATNMe$_6$ ligand are presented in Figures 12 and 13. Metrical data extracted from these voltammograms are summarized in Table 3. The data for the 2,2′-biquinoline[37] and the HATNMe$_6$ ligand[1c] have been previously reported but are reproduced here for comparison. Accurate $E_{1/2}$ values for $\mathbf{1}^{2+}$ have been derived from the DPV. The DPV measurements were initiated at the open circuit potential and performed separately toward positive and negative potentials. The free ligand 2,2′-biquinoline exhibits one reversible reduction step at −2.16 V, which is assigned to a one-electron addition to the lowest unoccupied molecular orbital (LUMO) to give $(\pi^*)^1$ electronic configuration.[38] A further irreversible reduction step can be assumed at approximately −2.65 V. The free hexaazatrinaphthylene ligand shows two reduction waves in the CV attributed to successive one-electron reduction steps at −1.55 and −1.89 V. The latter one is only reversible at high scan rates.

(36) Tebbe, K.-F. In *Homoatomic rings, chains, and macromolecules of main-group elements*; Rheingold, A. L., Ed.; Elsevier: Amsterdam, 1977; pp 551−606.
(37) Tabner, B. J.; Yandle, J. R. *J. Chem. Soc. A* **1968**, 381−388.
(38) Gyepes, R.; Witte, P. T.; Horacek, M.; Cisarova, I.; Mach, K. *J. Organomet. Chem.* **1998**, *551*, 207−213.

**Table 3.** Electrochemical Data for **1**, **2**, **3**, **4**, HATNMe$_6$ ($L_1$), and 2,2′-Biquinoline ($L_2$) (293 K, Solvent: $CH_3CN$ (**1**, **2**, **3**, **4**, $L_2$) and $CH_2Cl_2$ ($L_1$), 0.1 M $[(n\text{-}C_4H_9)_4N][PF_6]$)[a]

| added compound | | | $E_{1/2}$ values (V) |
|---|---|---|---|
| $\mathbf{1}^{2+}$ | couple I | $\mathbf{1}^{2-}/\mathbf{1}^-$ | −2.21 |
| | couple II | $\mathbf{1}^-/\mathbf{1}^0$ | −1.74 |
| | couple III | $\mathbf{1}^0/\mathbf{1}^+$ | −1.27 |
| | couple IV | $\mathbf{1}^+/\mathbf{1}^{2+}$ | −0.54 |
| | couple V | $\mathbf{1}^{2+}/\mathbf{1}^{3+}$ | −0.30 |
| | couple VI | $\mathbf{1}^{3+}/\mathbf{1}^{4+}$ | 0.11 |
| | couple VII | $\mathbf{1}^{4+}/\mathbf{1}^{5+}$ | 0.18 |
| | couple VIII | $\mathbf{1}^{5+}/\mathbf{1}^{6+}$ | 0.40 |
| HATNMe$_6$ ($L_1$) | couple I | $L_1^{2-}/L_1^-$ | −1.89 |
| | couple II | $L_1^-/L_1$ | −1.55 |
| $\mathbf{2}^+$ | couple I | $\mathbf{2}^-/\mathbf{2}$ | −1.86 |
| | couple II | $\mathbf{2}^0/\mathbf{2}^+$ | −1.32 |
| | couple III | $\mathbf{2}^+/\mathbf{2}^{2+}$ | −0.10 |
| $\mathbf{3}^+$ | couple I | $\mathbf{3}^-/\mathbf{3}$ | −1.91 |
| | couple II | $\mathbf{3}^0/\mathbf{3}^+$ | −1.39 |
| | couple III | $\mathbf{3}^+/\mathbf{3}^{2+}$ | −0.12 |
| $\mathbf{4}^+$ | couple I | $\mathbf{4}^-/\mathbf{4}$ | −1.50 |
| | couple II | $\mathbf{4}^0/\mathbf{4}^+$ | −0.89 |
| | couple III | $\mathbf{4}^+/\mathbf{4}^{2+}$ | 0.01 |
| 2,2′-biquinoline ($L_2$) | couple I | $L_2^{2-}/L_2^-$ | ∼ −2.65 |
| | couple II | $L_2^-/L_2$ | −2.16 |

[a] $E_{1/2}$ values are referenced versus the ferrocene/ferrocenium couple.

For each of the cationic mononuclear complexes $\mathbf{2}^+$−$\mathbf{4}^+$, two reversible reduction waves and one reversible oxidation wave are found in the potential region from ∼+1.8 to ∼−3.0 V versus the Fc/Fc$^+$ couple (Figure 12). The first reduction step is attributed to a one-electron reduction giving the corresponding neutral complex. The second reduction step is believed to be a ligand centered one-electron reduction. The oxidation wave arises from a one-electron oxidation of the titanium center, $3d^1 \rightarrow 3d^0$. The biquinoline complexes $\mathbf{2}^+$ and $\mathbf{3}^+$ reveal a very similar redox behavior in terms of their $E_{1/2}$ values and separations. In contrast, the voltammetric waves of the biquinoxaline complex $\mathbf{4}^+$ are noticeably shifted to higher potentials. Compared to the free biquinoline ligand, the reduction waves of $\mathbf{2}^+$, $\mathbf{3}^+$, and $\mathbf{4}^+$ are found at less negative potentials.

Since the trinuclear complexes $\mathbf{1}^{n+}$ are redox congeners, their voltammograms equal each other. Thus the voltammograms of $\mathbf{1}^{2+}$ are discussed as representative examples (Figure 13). $\mathbf{1}^{2+}$ was chosen due to its high solubility in acetonitrile. This allowed the investigation of 2 mM solutions resulting in acceptable ratios between Faradaic currents and double layer charging currents. The voltammograms exhibit four reduction waves as well as four oxidation waves (Figure 13). The first two reduction waves can be ascribed to well separated one-electron reductions leading to the redox congeners $\mathbf{1}^+$ and $\mathbf{1}^{\pm 0}$ (couples III and IV). The two further reduction waves assigned to one-electron reduction steps giving $\mathbf{1}^-$ and $\mathbf{1}^{2-}$ (couples I and II) are shifted to more negative potentials compared to those of the free HATNMe$_6$ ligand indicating that the acceptor capability of the HATNMe$_6$ unit decreases upon coordination of three titanocene synthons. This can be expected because of the reducing properties of titanocene. Comparable potential separations are found for the complex and the free ligand. The oxidation waves are attributed to stepwise one-electron oxidations leading to $\mathbf{1}^{3+}$, $\mathbf{1}^{4+}$, $\mathbf{1}^{5+}$, and $\mathbf{1}^{6+}$ (couples V−VIII). The

**Table 4.** Comproportionation Constants $K_c$ of the Mixed Valence States of **1** at 293 K

| compounds | $\Delta E_{1/2}$ (V)[a] | $K_c$[b] |
|---|---|---|
| $\mathbf{1}^-$ | 0.469 | $1.16 \times 10^8$ |
| $\mathbf{1}^+$ | 0.731 | $3.74 \times 10^{12}$ |
| $\mathbf{1}^{2+}$ | 0.243 | $1.52 \times 10^4$ |
| $\mathbf{1}^{4+}$ | 0.072 | 17.31 |
| $\mathbf{1}^{5+}$ | 0.212 | $4.50 \times 10^3$ |

[a] Separation between two adjacent half wave potentials representing the range wherein the respective compound exists. [b] Calculated by using the equation $\ln K_c = -nF\Delta E_{1/2}/RT$.

waves V, VI, VII, and VIII are found to be reversible at all scan rates. The couples VI and VII overlap. The resolution of the corresponding one-electron oxidation steps is achieved in the DPV enabling the determination of the $E_{1/2}$ values (Table 3).

The calculation of comproportionation constants $K_c$ provides valuable information about the electronic interaction characteristics between the titanium centers. The $K_c$ values are derived from the potential separation $\Delta E_{1/2}$ between couples ($\ln K_c = -nF\Delta E_{1/2}/RT$; $n$ = number of transferred electrons, $F$ = Faraday constant, $R$ = universal gas constant, and $T$ = temperature) and allow to evaluate the extent of electronic communication between the titanium centers.[39] The $K_c$ values of the mixed valence states $\mathbf{1}^-$, $\mathbf{1}^+$, $\mathbf{1}^{2+}$, $\mathbf{1}^{4+}$, and $\mathbf{1}^{5+}$ are given in Table 4. The comproportionation constants of the mixed valence states of **1** range between 17.3 ($\mathbf{1}^{4+}$) and $3.7 \times 10^{12}$ ($\mathbf{1}^+$). In the case of no electrochemical interaction, the $K_c$ value is 4 due to the statistical distribution of the compounds involved in the equilibrium.[40] The value of 17.3 obtained for $\mathbf{1}^{4+}$ displays a distribution close to the statistical one. Thus, electronic delocalization is limited and the metal centers are distinguishable and only weakly coupled. In contrast the value of $3.7 \times 10^{12}$ obtained for $\mathbf{1}^+$ is indicative of a strongly coupled system reflecting the high stabilization of the corresponding mixed valence state. On comparison to the $K_c$ of $\mathbf{1}^+$, the values for $\mathbf{1}^-$ ($K_c = 1.1 \times 10^8$) and $\mathbf{1}^{2+}$ ($K_c = 1.5 \times 10^4$) are smaller but nevertheless show evidence for pronounced electronic communication. The $K_c$ value found for $\mathbf{1}^{5+}$ ($K_c = 4.5 \times 10^3$) is indicative of a moderately coupled mixed valence system. The investigations on $\mathbf{1}^{n+}$ show that oxidation and reduction substantially affect the electronic interaction between the metal centers while structural changes are small. In addition one can derive from the $K_c$ values that, with exception of $\mathbf{1}^{4+}$, the complexes are stable with respect to disproportionation. In agreement $\mathbf{1}-\mathbf{1}^{3+}$ have been isolated as pure products as discussed in the previous chapter. The preparative syntheses of $\mathbf{1}^-$, $\mathbf{1}^{5+}$, and $\mathbf{1}^{6+}$ also should be feasible by employment of appropriate reductants and oxidants, respectively.

## Conclusions

In summary, we investigated the structure and redox behavior of cationic titanocene complexes with chelating *N*-heterocyclic ligand systems. As an additional characterization method, the ESI-MS technique has been applied. The syntheses of the cations were achieved by reaction of the neutral parents with ferrocenium salts as selective one-electron oxidants. The oxidation of the trinuclear HATN-type complex **1** enabled the isolation of four air-stable oxidation products $\mathbf{1}^+-\mathbf{1}^{4+}$ whereof $\mathbf{1}^+$, $\mathbf{1}^{2+}$, and $\mathbf{1}^{4+}$ are mixed valence compounds. The X-ray structural investigations revealed that only small structural changes occur upon oxidation. An increase of the Ti−Ti separation, an elongation of the Ti−N, and a contraction of the Ti−C bonds were observed as an effect of the electron abstraction. In all cases the $HATNMe_6$ ligand retained its planarity. The anion−$\pi$ interactions were found to affect the molecular arrangement of $\mathbf{1}^{2+}$, $\mathbf{1}^{3+}$, and $\mathbf{1}^{4+}$ in the crystal. The fluorine atoms of the counterions $PF_6^-$ and $BF_4^-$ revealed contacts to the $\pi$-acidic central ring of the HATN entity. In the case of $\mathbf{1}^{2+}$, this resulted in the assembly of an 1D polymer. The results of the CV and DPV investigations confirmed the structural stability of the redox congeners of **1**. Four oxidation waves and four reduction waves were found in the voltammograms of $\mathbf{1}^{2+}$. The stability of the mixed valence states of $\mathbf{1}^{n+}$ in solution has been determined by calculation of the respective comproportionation constants $K_c$. By this means, the redox congeners reveal weak ($\mathbf{1}^{4+}$), moderate ($\mathbf{1}^{5+}$), and strong ($\mathbf{1}^-$, $\mathbf{1}^+$, $\mathbf{1}^{2+}$) electronic metal−metal interaction, respectively. The voltammograms of the cations $\mathbf{2}^+-\mathbf{4}^+$ as mononuclear relatives of HATN-type cations exhibited one oxidation wave depicting the corresponding Ti(IV) complexes as well as two reduction waves. The crystal structures of $\mathbf{2}^+-\mathbf{4}^+$ revealed that structural changes, similar to those observed for the trinuclear compounds, occur upon oxidation of the neutral parents.

In conclusion, the first mixed valence titanocene complexes containing an *N*-heterocyclic ligand bridge have been presented from a synthetic, structural, and electrochemical point of view. Future studies will focus on the quantification of the electronic communication in the solid state. Therefore, magnetic measurements as well as NIR and Raman spectroscopic investigations in combination with theoretical considerations are in progress.

## Experimental Section

**Syntheses.** All operations were performed in a nitrogen atmosphere with rigorous exclusion of oxygen and moisture using glovebox and Schlenk techniques. Solvents were thoroughly dried and saturated with nitrogen. $[(Cp_2Ti)_3(\mu_3\text{-}HATNMe_6)]$ (**1**), $[(Cp_2Ti)(2,2'\text{-biquinoline})]$ (**2**), $[(Cp_2Ti)(4,4'\text{-dimethyl-}2,2'\text{-biquinoline})]$ (**3**), and $[(Cp_2Ti)(5,8'\text{-dimethyl-}2,3'\text{-biquinoxaline})]$ (**4**) have been prepared as described for analogous reactions[21] (see Supporting Information). $HATNMe_6$ was prepared according to the literature procedure.[1c] $[Cp_2Fe][PF_6]$ and $[Cp_2Fe][BF_4]$ were purchased from Aldrich and were used as received. EI and CI mass spectra were taken on a Finnigan-MAT 212 spectrometer. ESI mass spectrometric experiments were performed on a Finnigan LCQ (Thermo-Finnigan, San José, CA) quadrupole ion trap mass spectrometer or on a quadrupole time-of-flight Micromass Ultima Q-TOF instrument. IR spectra were recorded on a Bruker Vektor 22 spectrometer using

(39) (a) Richardson, D. E.; Taube, H. *Coord. Chem. Rev.* **1984**, *60*, 107−129. (b) Robin, M. B.; Day, P. *Adv. Inorg. Chem. Radiochem.* **1967**, *10*, 247−422. (c) Creutz, C. *Prog. Inorg. Chem.* **1983**, *30*, 1−73.
(40) Ward, M. D. *Chem. Soc. Rev.* **1995**, *24*, 121−134.

KBr pellets. Elemental analyses were carried out by the Analytischen Laboratorien (Lindlar, Germany).

**[$Cp_2Fe$][$BPh_4$].**[24c] Ferrocene (2.99 g, 16.1 mmol) was dissolved in sulfuric acid (60 mL, 96%). The dark blue solution was stirred for 20 min and was then diluted with water (600 mL) in an ice bath. The mixture was filtered and $NaBPh_4$ in water (300 mL) was added. A light blue solid precipitated immediately, which was isolated by filtration and thoroughly washed with cold water in small portions and subsequently with cold ethanol (3 × 30 mL) and diethylether (20 mL). The resulting light blue solid was dried in vacuo and stored at −25 °C under argon.

**[($Cp_2Ti$)$_3$($\mu_3$-HATNMe$_6$)][$BPh_4$] (1$^+$).** [($Cp_2Ti$)$_3$($\mu_3$-HATNMe$_6$)] (**1**) (200 mg, 0.2 mmol) and [$Cp_2Fe$][$BPh_4$] (101 mg, 0.2 mmol) were suspended in a mixture of *n*-hexane (25 mL) and THF (25 mL). The suspension was stirred overnight at room temperature. During the course of the reaction, the formation of a chartreuse, microcrystalline solid was observed. The solid was isolated by filtration, washed with *n*-pentane (20 mL), and subsequently dried in vacuo to yield a greenish powder (210 mg, 80%). Mp: 243−246 °C (dec). Anal. Calcd for $C_{84}H_{74}BN_6Ti_3$: C, 76.32; H, 5.64; N, 6.36. Found: C, 76.18; H, 5.73; N, 6.52. IR (KBr) $\tilde{\nu}$: 3052 (w), 3029 (w), 2979 (w), 2917 (w), 2853 (w), 1685 (w), 1579 (m), 1543 (s), 1468 (m), 1422 (s), 1361 (m), 1322 (m), 1287 (m), 1264 (m), 1220 (s), 1183 (m), 1115 (m), 1064 (w), 1013 (m), 809 (vs), 731 (m), 703 (s), 645 (m), 610 (m), 480 (w), 440 (w) cm$^{-1}$.

**[($Cp_2Ti$)$_3$($\mu_3$-HATNMe$_6$)][$PF_6$]$_2$ (1$^{2+}$).** [($Cp_2Ti$)$_3$($\mu_3$-HATNMe$_6$)] (**1**) (200 mg, 0.2 mmol) and [$Cp_2Fe$][$PF_6$] (132 mg, 0.4 mmol) were suspended in a mixture of *n*-hexane (15 mL) and THF (15 mL). The suspension was stirred overnight at room temperature. During the course of the reaction the formation of a yellow to orange precipitate was observed. The solid was isolated by filtration, washed with *n*-pentane (20 mL), and subsequently dried in vacuo to yield a yellow to orange powder (219 mg, 85%). Mp: >300 °C. Anal. Calcd for $C_{60}H_{54}F_{12}N_6P_2Ti_3$: C, 55.75; H, 4.21; N, 6.50. Found: C, 54.08 (lowered by TiC formation); H, 4.51; N, 6.39. IR (KBr) $\tilde{\nu}$: 3112 (w), 2919 (w), 2855 (w), 2726 (w), 2665 (w), 2587 (w), 1698 (w), 1625 (w), 1545 (m), 1487 (m), 1466 (m), 1362 (s), 1321 (s), 1224 (vs), 1185 (s), 118 (m), 1003 (m), 848 (vs), 639 (s), 605 (m), 556 (m), 501 (w), 478 (m), 445 (w) cm$^{-1}$.

**[($Cp_2Ti$)$_3$($\mu_3$-HATNMe$_6$)][$BF_4$]$_3$ (1$^{3+}$).** [($Cp_2Ti$)$_3$($\mu_3$-HATNMe$_6$)] (**1**) (200 mg, 0.2 mmol) and [$Cp_2Fe$][$BF_4$] (163 mg, 0.6 mmol) were suspended in a mixture of *n*-hexane (15 mL) and THF (15 mL). The suspension was stirred overnight at room temperature. During the course of the reaction, the formation of an orange precipitate was observed. The solid was isolated by filtration, washed with *n*-pentane (20 mL), and subsequently dried in vacuo to yield an orange powder (208 mg, 82%). Mp: slow decomposition above 150 °C. Anal. Calcd for $C_{60}H_{54}B_3F_{12}N_6Ti_3$: C, 57.05; H, 4.31; N, 6.65. Found: C, 56.59; H, 4.41; N, 6.74. IR (KBr) $\tilde{\nu}$: 3074 (w), 2918 (w), 2727 (w), 1625 (w), 1513 (w), 1485 (m), 1454 (m), 1365 (s), 1299 (w), 1228 (m), 1102 (s), 1035 (s), 829 (s), 748 (w), 533 (w), 521 (w), 502 (w), 451 (w) cm$^{-1}$.

**[($Cp_2Ti$)(2,2′-biquinoline)][$I_3$] (2$^+$$I_3^-$).** A solution of iodine (175 mg, 1.38 mmol) in toluene (50 mL) was slowly added to a stirred solution of [($Cp_2Ti$)(2,2′-biquinoline)] (**2**) (200 mg, 0.46 mmol) in toluene (30 mL) via a cannula. A green-brown solid precipitated immediately. After 10 min the solution was discolored. The solid was isolated by filtration, washed with *n*-pentane (30 mL), and subsequently dried in vacuo to yield a pale green powder (337 mg, 90%). Mp: 172 °C (decomposition). Anal. Calcd for $C_{28}H_{22}I_3N_2Ti$: C, 41.26; H, 2.72; N, 3.44. Found: C, 41.32; H, 2.76; N, 3.57. IR (KBr) $\tilde{\nu}$: 3087 (w), 3073 (w), 1616 (w), 1596 (m), 1508 (s), 1430 (m), 1375 (m), 1361 (m), 1210 (w), 1144 (m), 1096 (m), 1014 (s), 870 (w), 835 (w), 817 (s), 782 (w), 763 (w), 748 (m), 493 (w), 420 (w) cm$^{-1}$. MS (EI, 70 eV) *m*/*z* (%): 432 (10, [$Cp_2TiI_2$]$^+$), 305 (33, [$Cp_2TiI$]$^+$), 256 (100, [2,2′-biquinoline]$^+$), 178 (28, [$Cp_2Ti$]$^+$). MS (ESI, acetonitrile, positive scan) *m*/*z* (%): 434 (100, [($Cp_2Ti$)(2,2′-biquinoline)]$^+$). MS (ESI, acetonitrile, negative scan) *m*/*z* (%): 381 (32, [$I_3^-$]), 127 (100, [$I^-$]).

**[($Cp_2Ti$)(2,2′-biquinoline)][$PF_6$] (2$^+$$PF_6^-$).** [($Cp_2Ti$)(2,2′-biquinoline)] (**2**) (200 mg, 0.46 mmol) and [$Cp_2Fe$][$PF_6$] (152 mg, 0.46 mmol) were suspended in THF (30 mL). The suspension was stirred at room temperature for 12 h. During this time, a green precipitate formed which was isolated by filtration, washed with *n*-pentane (30 mL), and subsequently dried in vacuo to yield a green powder (224 mg, 84%). Mp: 188 °C (dec). Anal. Calcd for $C_{28}H_{22}F_6N_2PTi$: C, 58.05; H, 3.83; N, 4.84. Found: C, 57.82; H, 4.01; N, 4.67. IR (KBr) $\tilde{\nu}$: 3061 (w), 2925 (w), 1617 (m), 1599 (s),1552 (w), 1510 (s), 1455 (w), 1431 (s), 1375 (m), 1345 (w), 1283 (w), 1209 (m), 1142 (m), 1095 (m), 1014 (m), 950 (w), 847 (s), 785 (w), 759 (m), 557 (s), 512 (w), 495 (w), 419 (w) cm$^{-1}$. MS (CI, isobutane) *m*/*z* (%): 434 (23, [($Cp_2Ti$)(2,2′-biquinoline)]$^+$), 257 (100, [2,2′-biquinoline + H$^+$]), 178 (4, [$Cp_2Ti$]$^+$). MS (ESI, acetonitrile, positive scan) *m*/*z* (%): 434 (100, [($Cp_2Ti$)(2,2′-biquinoline)]$^+$). MS (ESI, acetonitrile, negative scan) *m*/*z* (%): 145 (100, [$PF_6^-$]).

**[($Cp_2Ti$)(4,4′-dimethyl-2,2′-biquinoline)][$PF_6$] (3$^+$).** [($Cp_2Ti$)-(4,4′-dimethyl-2,2′-biquinoline)] (**3**) (200 mg, 0.43 mmol) and [$Cp_2$-Fe][$PF_6$] (143 mg, 0.43 mmol) were suspended in THF (30 mL). The suspension was stirred at room temperature, and the formation of a green precipitate was observed. After 4 h, the solid was isolated by filtration, washed with *n*-pentane (30 mL), and subsequently dried in vacuo to yield a green powder (194 mg, 74%). Mp: 222−228 °C (dec). Anal. Calcd for $C_{30}H_{26}F_6N_2PTi$: C, 59.32; H, 4.31; N, 4.61. Found: C, 58.65; H, 4.39; N, 4.76. IR (KBr) $\tilde{\nu}$: 3122 (w), 2980 (w), 1599 (s), 1518 (s), 1453 (m), 1415 (m), 1380 (m), 1368 (m), 1326 (w), 1221 (w), 1164 (w), 1107 (m), 1013 (w), 914 (w), 847 (s), 768 (s), 707 (w), 557 (s), 430 (w) cm$^{-1}$. MS (EI, 70 eV) *m*/*z* (%): 462 (3, [($Cp_2Ti$)(4,4′-dimethyl-2,2′-biquinoline)]$^+$), 284 (100, [4,4′-dimethyl-2,2′-biquinoline]$^+$), 178 (5, [$Cp_2Ti$]$^+$). MS (ESI, acetonitrile, positive scan) *m*/*z* (%): 462 (100, [($Cp_2Ti$)(4,4′-dimethyl-2,2′-biquinoline)]$^+$). MS (ESI, acetonitrile, negative scan) *m*/*z* (%): 145 (100, [$PF_6^-$]).

**[($Cp_2Ti$)(5,8′-dimethyl-2,3′-biquinoxaline)][$PF_6$] (4$^+$).** [($Cp_2$-Ti)(5,8′-dimethyl-2,3′-biquinoxaline)] (**4**) (200 mg, 0.43 mmol) and [$Cp_2Fe$][$PF_6$] (143 mg, 0.43 mmol) were suspended in THF (30 mL). The suspension was stirred for 4 h at room temperature. Within this time, a greenish, microcrystalline solid was formed, which was isolated by filtration, washed with *n*-pentane (30 mL), and subsequently dried in vacuo to yield a green powder (197 mg, 75%). Mp: 184 °C (dec). Anal. Calcd for $C_{28}H_{24}F_6N_4PTi$: C, 55.19; H, 3.97; N, 9.19. Found: C, 54.86; H, 4.13; N, 9.37. IR (KBr) $\tilde{\nu}$: 3116 (w), 2962 (w), 2924 (w), 1608 (w), 1575 (w), 1535 (w), 1497 (m), 1467 (m), 1435 (m), 1363 (m), 1345 (s), 1204 (m), 1142 (s), 1012 (m), 987 (m), 910 (w), 852 (vs), 777 (m), 557 (s), 486 (w), 453 (w) cm$^{-1}$. MS (EI, 70 eV) *m*/*z* (%): 464 (40, [($Cp_2Ti$)(5,8′-dimethyl-2,3′-biquinoxaline)]$^+$), 286 (100, [5,8′-dimethyl-2,3′-biquinoxaline]$^+$), 178 (38, [$Cp_2Ti$]$^+$). MS (ESI, acetonitrile, positive scan) *m*/*z* (%): 464 (100, [($Cp_2Ti$)(5,8′-dimethyl-2,3′-biquinoxaline)]$^+$). MS (ESI, acetonitrile, negative scan) *m*/*z* (%): 145 (100, [$PF_6^-$]).

**Electrochemistry.** CV and DPV were recorded using a CHI 620B potentiostat (CH Instruments, Austin, TX). The electrochemical cell consisted of a Pt disk working electrode, a Pt wire counter electrode, and a single-unit Haber−Luggin capillary/dual reference electrode system.[41] Experiments were conducted at room temperature in purified acetonitrile and $CH_2Cl_2$ (HATNMe$_6$) using 0.1 M

**Table 5.** Crystal Structure Data for Compounds $\mathbf{1}^+$, $\mathbf{1}^{2+}$, $\mathbf{1}^{3+}$, $\mathbf{2}^+\mathbf{PF_6}^-$, $\mathbf{3}^+$, and $\mathbf{2}^+\mathbf{I_3}^-$

| | $\mathbf{1}^+$ | $\mathbf{1}^{2+}$ | $\mathbf{1}^{3+}$ | $\mathbf{2}^+\mathbf{PF_6}^-$ | $\mathbf{3}^+$ | $\mathbf{2}^+\mathbf{I_3}^-$ |
|---|---|---|---|---|---|---|
| empirical formula | $C_{112}H_{130}BN_6O_7Ti_3$ | $C_{69}H_{72}F_{12}N_6O_3P_2Ti_3$ | $C_{72}H_{78}B_3F_{12}N_6O_4Ti_3$ | $C_{28}H_{22}F_6N_2PTi$ | $C_{30}H_{26}F_6N_2PTi$ | $C_{28}H_{22}I_3N_2Ti$ |
| fw | 1826.68 | 1466.97 | 1495.53 | 579.35 | 607.40 | 815.08 |
| color habit | dark cuboids | dark plates | orange plates | green cuboids | green plates | brown-green plates |
| cryst size, mm | 0.68 × 0.13 × 0.04 | 0.2 × 0.13 × 0.03 | 1.2 × 0.26 × 0.11 | 0.20 × 0.10 × 0.07 | 0.50 × 0.21 × 0.13 | 0.20 × 0.16 × 0.12 |
| crystal syst | orthorhombic | monoclinic | monoclinic | orthorhombic | monoclinic | orthorhombic |
| space group | *Pbca* | $P2_1/n$ | $P2_1/c$ | *Pbca* | $P2_1/c$ | *Pbcn* |
| *a*, Å | 22.3769(6) | 16.3898(7) | 15.4273(7) | 15.1450(5) | 10.8817(6) | 8.1348(2) |
| *b*, Å | 28.1718(10) | 14.8294(9) | 30.339(2) | 19.5690(12) | 17.8329(5) | 16.9495(5) |
| *c*, Å | 30.5731(13) | 28.2782(11) | 14.7438(5) | 16.5042(6) | 14.3651(6) | 19.2166(9) |
| α, deg | 90 | 90 | 90 | 90 | 90 | 90 |
| *β*, deg | 90 | 90.054(5) | 99.948(5) | 90 | 111.953(5) | 90 |
| *γ*, deg | 90 | 90 | 90 | 90 | 90 | 90 |
| *V*, Å$^3$ | 19273.2(12) | 6873.0(6) | 6797.1(6) | 4891.4(4) | 2585.45 (19) | 2649.60(16) |
| *Z* | 8 | 4 | 4 | 8 | 4 | 4 |
| $D_{calc}$, g cm$^{-3}$ | 1.259 | 1.418 | 1.461 | 1.573 | 1.560 | 2.043 |
| $\mu$, mm$^{-1}$ | 0.303 | 0.470 | 0.432 | 0.483 | 0.461 | 3.838 |
| *T*, K | 153(2) | 153(2) | 153(2) | 153(2) | 153(2) | 153(2) |
| $\theta$ range, deg | 2.07−26.13 | 1.99−26.07 | 2.21−26.12 | 2.42−26.09 | 2.32−26.16 | 2.12−26.09 |
| reflns collected | 166643 | 55761 | 65227 | 40871 | 25542 | 23745 |
| independent reflns | 18269 ($R$(int) = 0.2325) | 12711 ($R$(int) = 0.2653) | 12619 ($R$(int) = 0.0682) | 4827 ($R$(int) = 0.1292) | 4919 ($R$(int) = 0.0470) | 2610 ($R$(int) = 0.0462) |
| reflns with $I > 2\sigma(I)$ | 6948 | 3843 | 8145 | 2545 | 3820 | 1995 |
| abs correction | numerical | none | numerical | none | numerical | numerical |
| max and min transm | 0.9880 and 0.8204 | 0.9860 and 0.9119 | 0.9540 and 0.6251 | 0.9670 and 0.9096 | 0.9425 and 0.8023 | 0.6559 and 0.5140 |
| final *R* indices ($I > 2s(I)$) | R1 = 0.0819 wR2 = 0.1931 | R1 = 0.1205 wR2 = 0.2881 | R1 = 0.0516 wR2 = 0.1376 | R1 = 0.0440 wR2 = 0.0836 | R1 = 0.0431 wR2 = 0.1098 | R1 = 0.0179 wR2 = 0.0373 |
| *R* indices (all data) | R1 = 0.1837 wR2 = 0.2354 | R1 = 0.2606 wR2 = 0.3355 | R1 = 0.0836 wR2 = 0.1544 | R1 = 0.1012, wR2 = 0.0969 | R1 = 0.0565 wR2 = 0.1151 | R1 = 0.0298 wR2 = 0.0391 |

$[(n\text{-}C_4H_9)_4N][PF_6]$ as the supporting electrolyte. All potentials are referred to the half wave potential of the ferrocene/ferrocenium couple measured in the same setup. The CV and DPV were initiated at the open circuit potential. The pulse amplitude $\Delta E$ in DPV measurements was varied between 10 and 50 mV. The $E_{1/2}$ values quoted in Table 3 were determined from the peak potentials $E_p$ of the DPV.[42] The experimentally observed $E_p$ values for each signal were plotted as function of $\Delta E$. The extrapolation of the function $E_p = E_{1/2} - \Delta E/2$ for $\Delta E \rightarrow 0$ yields $E_{1/2}$.

**X-ray Structure Determination.** Crystals of $\mathbf{1}^+$, $\mathbf{1}^{2+}$, $\mathbf{1}^{3+}$, $\mathbf{1}^{4+}$, $\mathbf{2}^+\mathbf{PF_6}^-$, $\mathbf{2}^+\mathbf{I_3}^-$, and $\mathbf{3}^+$ suitable for X-ray structure analysis were grown by slow diffusion of *n*-pentane into a THF solution of $\mathbf{1}^+$ and by slow diffusion of *n*-pentane into acetone solutions of $\mathbf{1}^{2+}$, $\mathbf{1}^{3+}$, $\mathbf{1}^{4+}$, $\mathbf{2}^+\mathbf{PF_6}^-$, $\mathbf{2}^+\mathbf{I_3}^-$, and $\mathbf{3}^+$, respectively. Crystals of $\mathbf{4}^+$ were obtained by recrystallization from acetone. Single-crystal experiments were carried out on a Stoe IPDS diffractometer with graphite monochromated Mo Kα radiation ($\mu$ = 0.71073 Å). All structures were solved by direct phase determination and refined by full-matrix least-squares techniques against $F^2$ with the SHELXL-97 program system.[43] Crystallographic details of $\mathbf{1}^{4+}$ and $\mathbf{4}^+$ are given in the Supporting Information since the respective crystals only allowed collection of low quality X-ray data sets. However, determination of connectivities was possible. Data for $\mathbf{1}^+$, $\mathbf{1}^{2+}$, $\mathbf{1}^{3+}$, $\mathbf{1}^{4+}$, $\mathbf{2}^+\mathbf{I_3}^-$, $\mathbf{2}^+\mathbf{PF_6}^-$, $\mathbf{3}^+$, and $\mathbf{4}^+$ have been deposited with the Cambridge Crystallographic Data Centre: CCDC-627764 $\mathbf{1}^+$, CCDC-635827 $\mathbf{1}^{2+}$, CCDC-627766 $\mathbf{1}^{3+}$, CCDC-627765 $\mathbf{1}^{4+}$, CCDC-627763 $\mathbf{2}^+\mathbf{I_3}^-$, CCDC-627768 $\mathbf{2}^+\mathbf{PF_6}^-$, CCDC-627767 $\mathbf{3}^+$, CCDC-635826 $\mathbf{4}^+$. Crystallographic details are give in Table 5. Details for the neutral complexes **3** (CCDC-639535) and **4** (CCDC-639534) are give in the Supporting Information.

**Acknowledgment.** We thank the Fonds der Chemischen Industrie for a kindly granted scholarship (I.P.) and the Deutsche Forschungsgemeinschaft for support. We also thank Bernd Speiser, University of Tübingen, for the expert advice regarding the reference electrode system.

**Supporting Information Available:** X-ray crystallographic files, syntheses and chemical structures for **3** and **4**, and ESI-MS data. This material is available free of charge via the Internet at http://pubs.acs.org.

IC701009U

(41) Gollas, B.; Krauss, B.; Speiser, B.; Stahl, H. *Curr. Sep.* **1994**, *13* (2), 42−44.
(42) Bard, A. J.; Faulkner, L. R. *Electrochemical Methods: Fundamentals and Applications*, 2nd ed.; John Wiley & Sons: New York, 2001.
(43) Sheldrick, G. M. *SHELXL-97, A Program for Refining Crystal Structures*; University of Göttingen: Germany, 1997.